Crystallographic orientation dependence of ferroelectric domain walls in antiferroelectric lead zirconate thin films

Mamadou Coulibaly, Caroline Borderon, Raphaël Renoud, Hartmut Gundel

Crystallographic orientation dependence of ferroelectric domain walls in antiferroelectric lead zirconate thin films

Mamadou D. Coulibaly[1], Caroline Borderon[1], Raphaël Renoud[1,*] and Hartmut W. Gundel[1]

[1] *IETR UMR CNRS 6164, University of Nantes, 2 Rue de la Houssinière, 44322 Nantes*

*corresponding author e-mail: mamadoucoulibalypro1@gmail.com

Keywords: Antiferroelectric, domain walls, Ti seed layer,

Abstract—

In this study, two antiferroelectric $PbZrO_3$ samples with a (100) preferential orientation and with two different crystallographic directions ((100) and (111)) have been studied. The sample with the (111) direction has a higher polarization and lower field transitions due to the reduction of the angle between the applied electric field and the ferroelectric polar axis ($\vec{P}_{FE}$). The study of the permittivity reveals also that this sample has a higher correlation of dipoles ($|S_{hf}| = 0.007$) due to the energy gain associated with their orientation. The dielectric response of the domain walls in the differently oriented $PbZrO_3$ are then identical because they have the same environment (same grain size and similar defects in the two samples) and interact in the same way. Only the domain wall density is higher in the $PbZrO_3$ with different crystallographic directions due to the inhomogeneity of the crystallization orientation, which creates more nucleation site for domain walls.

Introduction

Ferroelectric materials are increasingly being considered as critical components in next generation nonvolatile memories [1], actuators and energy storage devices [2],[3]. For the last applications, it is necessary to have a great polarization and a low switching field between the antiferroelectric and ferroelectric phase. Low dielectric losses and high permittivity are also required. Recently, ferroelectric domain walls into small ferroelectric clusters have been located in antiferroelectric phase. This domain walls created supplementary dielectric losses and may disadvantage the desired application. A deep understanding of the ferroelectric domain walls motions will then helpful to understand how limited the losses due to this ferroelectric domain walls. Previous studies on ferroelectric materials have been shown that domains response can be tuned by modifying the crystallographic orientation of thin films [4],[5]. However, no study on domain walls have been done on crystallographic orientations on antiferroelectric materials and most of the previous studies are focused on epitaxial single-crystalline thin films. The important influence of crystallographic orientation in polycrystalline films has not been studied while these are highly interesting for optimizing devices in a low cost way.

In this study, the influence of the crystallographic orientation on the ferroelectric phase of antiferroelectric $PbZrO_3$ thin films are studied. Two samples with different crystallographic orientation have been done with a simple and low cost sol-gel way. The polarization versus electric field has been measured and domain wall motions are studied by using a hyperbolic law based on Rayleigh analysis, which consist to measure the permittivity as a function of the amplitude of a low electric field. All parameters have been compared to conclude on the influence of crystallographic orientation on ferroelectric domain wall motions.

Experimental procedure

The samples are prepared by a sol-gel process detailed elsewhere [3]. The precursor solution has been deposited at 4000 rpm during 25 s by a multi-step spin coating process on a polished alumina substrate. This substrate has been precoated with a 40 nm titanium adhesion layer and a 300 nm platinum bottom layer done by magnetron sputtering. Twelve layers have been deposited and each layer was annealed during 10 min in a pre-heated open air furnace at 650°C. The overall $PbZrO_3$ films thickness is 800 nm. To modify the crystallographic orientation of the thin layers, a 2nm Ti seed layer has been deposited on the platinum layer of one sample before the deposition of the solution [3]. This permits us to reduce the lattice mismatch between the Pt electrode and the $PbZrO_3$ films [3]. The structure and phase purity of the films were analyzed using a *Bruker D8*X- ray diffractometer (XRD) with Cu$K\alpha$ radiation. All samples are well crystallized and the indices of the pseudocubic perovskite structure are mentioned in Fig.1. No parasitic phase is present. The orientation factor of the $PbZrO_3$ thin films $\alpha_{hkl} = I_{hkl}/I_{total}$ [6-7] has been calculated taking into account effects of structure and atomic form factors. I_{hkl} corresponds to the peak intensity of the selected plane and I_{total} is the sum of all diffraction peaks. The lead zirconate thin films without Ti seed layer are oriented along the (100) crystallographic plane at around 99 %. This orientation on polycrystalline alumina substrate is due to a most thermodynamically favorable growth direction [8-9] on a lowest surface energy [10]. Thanks to the use of a Ti seed layer, the $PbZrO_3$ films are oriented along the (111) direction at 70 %. During the annealing process, the Ti seed layer forms an intermetallic (Pt_3Ti) layer with the platinum bottom electrode [10-11], reducing the lattice mismatch between the (111) oriented platinum bottom electrode and the $PbZrO_3$ thin films [3]. Thus, we have two samples with two crystallographic configurations: one highly oriented in the (100) direction and the other with a preferential orientation in the (111) direction but with other orientations.

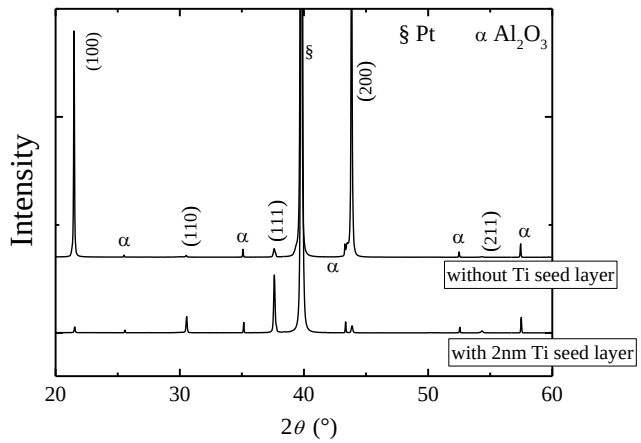

Fig 1. X-ray diffraction patterns of the lead zirconate thin films with and without a Ti seed layer.

Square platinum electrodes of 0.5 mm broad were then deposited by RF magnetron sputtering in order to realize a Metal-Insulator-Metal (MIM) capacitor. The polarization versus electric field (*P–E*) hysteresis loops and the current - electric field (*I–E*) hysteresis loops were measured at 1kHz using a classical Sawyer Tower circuit. The capacitance and the dielectric losses (tan δ) were measured with an *Agilent 4294A*. The real and imaginary parts of the

permittivity have been calculated from the capacitance and the dielectric loss values. The variation of the permittivity has been measured as a function the AC field amplitude (0.6 kV/cm to 12.5 kV/cm corresponding to an applied voltage from 5 mV to 1 V, respectively). All the measurements were performed at room temperature (20 °C).

Results and discussion

Polarization loops of the lead zirconate thin films at 600 kV/cm are shown in the Fig.2a. Both films present a double hysteresis loops, indicating their antiferroelectric nature but the $PbZrO_3$ with different orientation presents a higher maximum polarization (36 μC/cm^2) than the (100) $PbZrO_3$ (23 μC/cm^2). This difference is due to the modification of the polar axis orientation. For (111) oriented $PbZrO_3$ thin films, the angle θ between the direction of the applied electric field ($\vec{E}$) and the [111] polar axis ($\vec{P}_{FE}$) of the ferroelectric rhombohedral phase is lower compared to the (100) $PbZrO_3$ configuration [10-12] (Fig. 3). Thus, the projection of the polarization along the direction of the electric field applied is greater for the (111) $PbZrO_3$ thin films. Consequently, the $PbZrO_3$ samples with a preferential orientation in the (111) direction has a higher polarization than the (100) $PbZrO_3$.

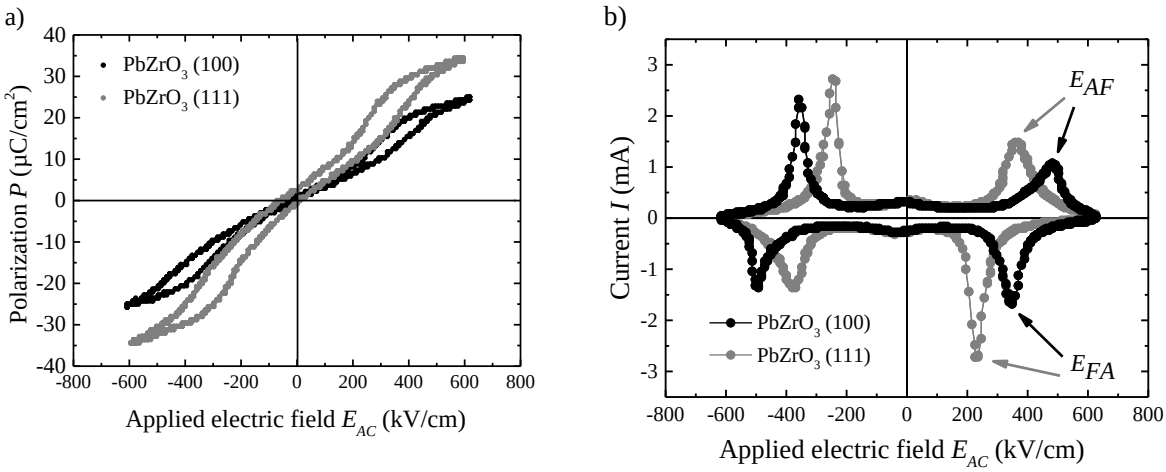

Fig. 4. a) Polarization and b) current – electric hysteresis loops of (100) and (111) lead zirconate thin films at 1kHz. E_{AF} and E_{FA} are the transitions fields.

Current – electric field loops of the two $PbZrO_3$ samples are shown in Fig.2b. The switching current curves have four peaks corresponding to the antiferroelectric–ferroelectric fields E_{AF} and to ferroelectric–antiferroelectric E_{FA} field transitions for positive and negative field. The $PbZrO_3$ with different orientation presents a lower antiferroelectric-ferroelectric field transition (E_{AF} = 340 kV/cm) than the (100) $PbZrO_3$ (E_{AF}= 480 kV/cm). This behavior is also induced by the reduction of the angle θ between the applied electric field and the ferroelectric polar axis ($\vec{P}_{FE}$). As θ is low, the energy necessary to align the dipoles in the direction of the electric field is smaller. Therefore, the $PbZrO_3$ with a preferential orientation in the (111) direction is easier to polarize compared to the (100) $PbZrO_3$. For this reason, it also has a lower ferroelectric-antiferroelectric transition field (E_{FA}= 220 kV/cm) than the (100) $PbZrO_3$ (E_{FA}= 340 kV/cm). Near zero electric field, the current *I* slightly increases and indicates the existence of a residual ferroelectric phase in the antiferroelectric state, which is not visible on the *P-E* loop. This phenomenon is common for pure lead zirconate ($PbZrO_3$) [13-14] due to an unbalanced antiparallel shift of the oxygen atoms along the [001] direction and is attributed to the coexistence of ferroelectric and antiferroelectric phonon modes [13-14].

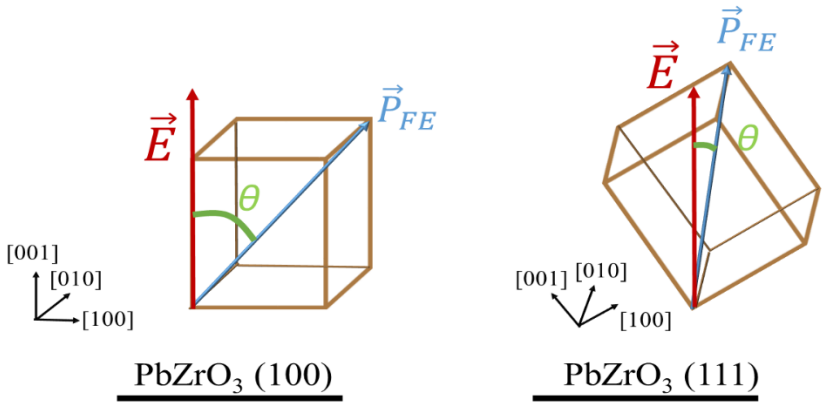

Fig. 3. Schematic diagram of the primitive cells for the (100) and (111) oriented $PbZrO_3$, where θ is the angle between the applied electric field $\vec{E}$ and the ferroelectric polar axis $\overrightarrow{P_{FE}}$

In order to study this residual ferroelectric phase for the two types of $PbZrO_3$ thin films, the permittivity was measured at different frequencies as a function of the amplitude of the exciting electric field (Fig.4). For both samples, the permittivity increases when the driving electric field increases indicating ferroelectric domain wall motion [15-16] as antiferroelectric domain wall motion cannot appear under the action of a homogeneous electric field [17]. The evolution of the permittivity can be describe as a function of the amplitude of the exciting electric field ($E_{AC} \ll$ transition field E_{AF}) by a hyperbolic law [15]:

$$\varepsilon_r = \varepsilon_{rl} + \sqrt{{\varepsilon_{r-rev}}^2 + (\alpha_r E_{AC})^2}\,. \qquad (1)$$

This law permits us to determine the contribution ε_{r-rev} from domain walls vibration (reversible contribution), α_r from domain walls pinning/unpinning (irreversible contribution) and the contribution from the lattice ε_{rl} [15-18]. Therefore, no term related to the presence of antiferroelectric domain walls appears in the hyperbolic law. The electric field E_{AC} is very low comparing to E_{AF}, so, no switching polarization occurs and the domain wall density remains constant during the measurement [17].

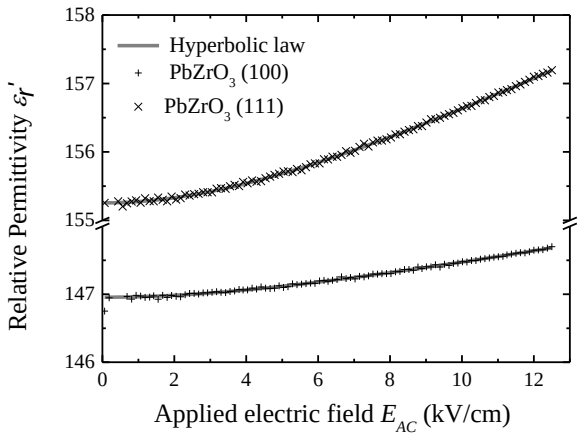

Fig. 4. The real part of relative permittivity is plotted against applied AC electric field E_{AC} (black crosses) for the (100) and (111) oriented $PbZrO_3$. The solid grey line is a fit to the hyperbolic law (equation 1) at 1 kHz.

To study ferroelectric domain wall motions, the different parameters were measured and calculated from equation (1) at different frequencies. Fig. 5 shows the real and imaginary part of the lattice contribution ε_{rl} as a function of frequency. The evolution of the permittivity is fitted using the "universal power law" (demonstrated by Jonscher [19]) which described any dielectric relaxation in solids. In our case, two relaxation phenomena are superposed, one occurring at higher frequencies than the other [3]:

$$\varepsilon_{rl} = \varepsilon_{hf}\,\omega^{S_{hf}} + \varepsilon_{lf}\,\omega^{S_{lf}}. \qquad (2)$$

ε_{hf} and ε_{lf} are respectively the permittivity contribution at "high" and "low" frequencies, $\varepsilon_{hf}\,\omega^{S_{hf}}$ and $\varepsilon_{lf}\,\omega^{S_{lf}}$ represent respectively the high frequency relaxation and the low frequency diffusion [19]. Fitting of the experimental data (least squares method) is presented in Fig.5 and the coefficients are given in Table 1. According to the invariance of a power law by Hilbert transformation (Kramer-Kronig relations), exponents of the two contributions are the same for the real and the imaginary part of the permittivity [3], only weighting coefficients vary.

The two samples present a similar real permittivity of the lattice at high frequencies but the decrease of the permittivity in the range [1 kHz – 1 MHz] is higher for the $PbZrO_3$ with a preferential orientation in the (111) direction. This difference is essentially due to the low diffusion frequency (table 1). The exponent S_{lf} (-0.40) of the (100) $PbZrO_3$ is identical to those obtained for ferroelectric oxides [3-20] whereas it is only equal to -0.2 for the $PbZrO_3$ with a preferential orientation in the (111) direction. In ferroelectric oxides, oxygen vacancies leave dangling bonds [21] which allows hopping of electrons [22] as shown in lead zirconate thin films [23]. This mechanism, due only to the presence of oxygen vacancies, explains why the exponent S_{lf} takes the same value for different ferroelectric oxides [3-20]. For the $PbZrO_3$ with a preferential orientation in the (111) direction, oxidation of the Ti seed layer generates supplementary defects by increasing the generation of oxygen vacancies and its exponent S_{lf} (-0.20) is different. However, S_{lf} exponent values between -0.2 and -0.4 are often associated with hopping conduction [22].

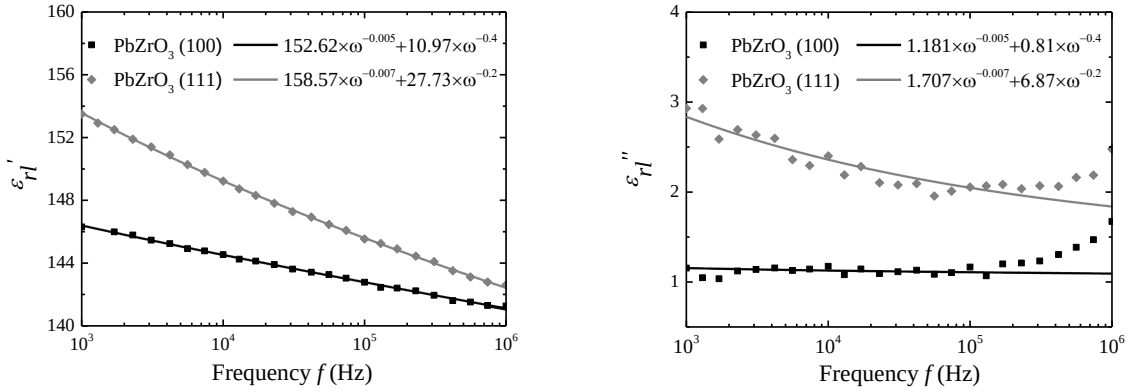

Fig. 5. Real and imaginary part of the lattice contribution to the permittivity as a function of frequency, decomposed according to the hyperbolic law (equation 2). Evolution of the lattice contribution is fitted with the equation 3. The increase of the losses above 10^5 Hz is due to a resonance of the impedance analyzer.

	High frequency relaxation				Low frequency diffusion			
	S_{hf}	ε'_{hf}	ε''_{hf}	$\tan\delta_{hf}$	S_{lf}	ε'_{lf}	ε''_{lf}	$\tan\delta_{lf}$
$PbZrO_3$ (100)	-0.005 ± 0.001	152.6 ± 0.1	1.18 ± 0.01	0.007 ± 0.001	-0.40 ± 0.01	10.97 ± 0.01	0.81 ± 0.01	0.073 ± 0.001

$PbZrO_3$ (111)	-0.007 ± 0.001	158.5 ± 0.1	1.71 ± 0.01	0.011 ± 0.001	-0.20 ± 0.01	27.73 ± 0.01	6.87 ± 0.01	0.247 ± 0.001

Table 1. Exponents, weighting coefficients and dissipation factors of the lattice contribution to the permittivity.

For the high frequency relaxation, the coefficient of the (100) PbZrO3 are slightly smaller than for the $PbZrO_3$ with a preferential orientation in the (111) direction. In this case, the exponent S_{hf} is attributed to the relaxation of the dipoles. According to Jonscher [19-22], $|S_{hf}|$ accounts for the importance of the correlations between the dipoles and are favored when the mutual influence due to the electric field generate by dipoles is important [3]. The system is completely correlated when $|S_{hf}| = 1$ and $|S_{hf}| = 0$ when the system does not admit any correlation. Therefore, for the $PbZrO_3$ with a preferential orientation in the (111) direction, by lowering the energy necessary to head-to-tail dipoles (antiferroelectric state) to switch to parallels dipoles (ferroelectric state), a higher correlation of dipoles is obtained ($|S_{hf}| = 0.007$) due to the energy gain associated with the orientation of dipoles. While for (100) $PbZrO_3$, a lower value is obtained ($|S_{hf}| = 0.005$) $PbZrO_3$ due to the higher energy necessary (higher transition field E_{AF}) for the transitions of head-to-tail dipoles.

Dissipation factor of the low and high frequency components, $\tan \delta_{hf} = \varepsilon''_{hf} / \varepsilon'_{hf}$ and $\tan \delta_{lf} = \varepsilon''_{lf} / \varepsilon'_{lf}$ are also calculated (Table 1). Due to the oxidation of the Ti seed layer, which generates supplementary defects, dissipation factors of the $PbZrO_3$ with a preferential orientation in the (111) direction are more important. A previous study [20] has shown that the presence of oxygen vacancies is the origin of the high dissipative factor at low frequencies [20] and the compensation of theses vacancies leads to the reduction of dissipation factors.

The contribution due to domain wall motions are difficult to obtain because of their low contribution (lower than 1 %) to the permittivity. Fig. 6 and Fig. 7 show real and imaginary part of the vibration and domain wall pinning contributions to the permittivity as a function of frequency for the two PZO samples. Their evolutions are fitted with a power law [3]:

$$\varepsilon_{r\text{-}rev} = \varepsilon_{f\text{-}rev}\, \omega^{S_{rev}}, \tag{4}$$

$$\alpha_r = \alpha_f\, \omega^{S_\alpha}, \tag{5}$$

where $\varepsilon_{f\text{-}rev}$ and α_f represent respectively the vibration and the pinning/unpinning contributions at ω = 1 rad/s, S_{rev} and S_α their frequency dependence. In order to respect the Kramer-Kronig relations [24Kev], the exponent are the same for real and imaginary part of $\varepsilon_{r\text{-}rev}$ and α_r. Coefficients and dissipation factors are given in Table 2. The real part of the vibration $\varepsilon'_{f\text{-}rev}$ and the pinning/unpinning α_f coefficients of the $PbZrO_3$ with different orientations is 2.8 times higher compared to the (100) $PbZrO_3$. This two coefficients are proportional to the domain wall density [20]. The $PbZrO_3$ with different crystallographic direction has more obstacles due to the inhomogeneity of the crystallization orientation and consequently has more nucleation site and a higher domain walls density. However, independently to their crystallographic orientations, domain walls motions of the (100) $PbZrO_3$ and the $PbZrO_3$ with different orientations present the same frequency dependence S_{rev} and S_α. Even if the orientations of the two samples are different, the conditions of crystallization are identical. The differently oriented domain walls thus have the same environment (same grain size and similar defects in the two samples) and interact in the same way. Moreover, the coefficient S_α is higher than the coefficient S_{rev}, which indicates that the irreversible (pinning/unpinning) phenomenon cannot follow the switching field at high frequencies.

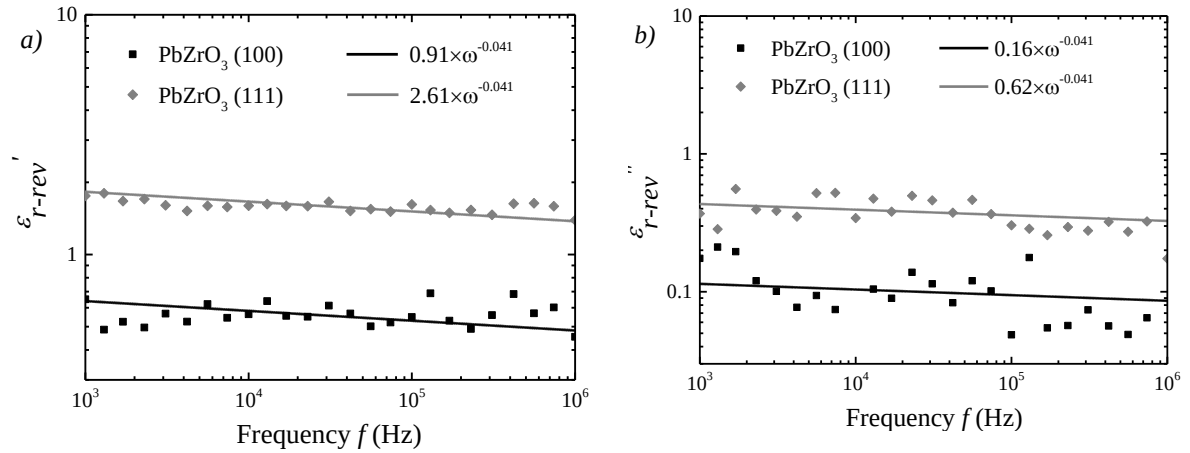

Fig. 6. a) Real and b) imaginary part of the domain wall vibrations contribution to the permittivity as a function of frequency, decomposed according to the hyperbolic law (equation 1) and fitted with equation 4.

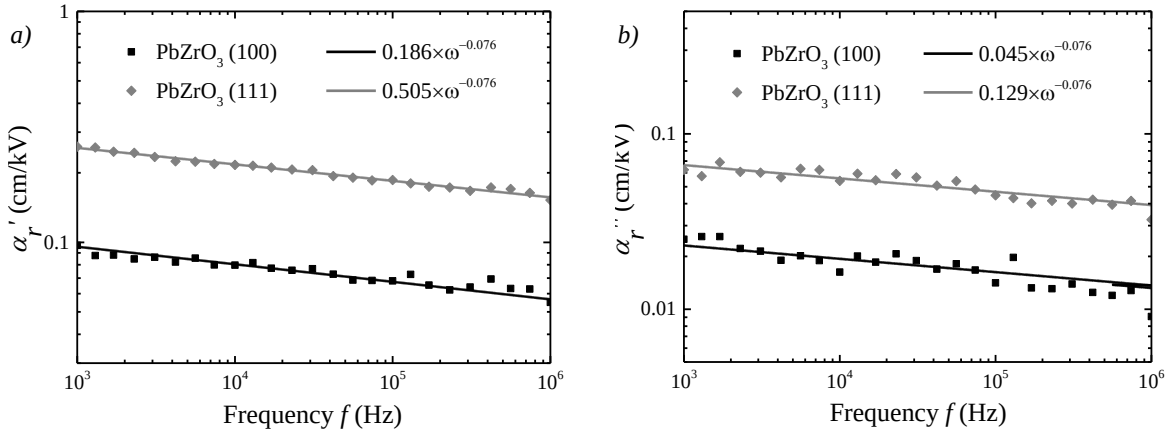

Fig.7. a) Real and b) imaginary part of the domain wall pinning contribution to the permittivity as a function of frequency, decomposed according to the hyperbolic law (equation 2) and fitted with equation 4.

	S_{rev}	ε'_{f-rev}	ε''_{f-rev}	m_{rev}	S_α	α'_f (cm/kV)	α''_f (cm/kV)	m_α	E_{th} (kV/cm)
$PbZrO_3$ (100)	-0.04 ± 0.01	0.91 ± 0.01	0.16 ± 0.01	0.17 ± 0.01	-0.076 ± 0.005	0.186 ± 0.005	0.045 ± 0.005	0.23 ± 0.04	4.9 ± 0.2
$PbZrO_3$ (111)	-0.04 ± 0.01	2.61 ± 0.01	0.62 ± 0.01	0.23 ± 0.01	-0.076 ± 0.005	0.505 ± 0.005	0.129 ± 0.005	0.25 ± 0.04	5.1 ± 0.2

Table 2. Exponents, weighting coefficients and dissipation factors of the vibrations and domain wall pinning contribution to the permittivity.

To compare the two coefficients of domain wall motions, the threshold field of domain wall pinning (E_{th}) is calculated by [15]:

$$E_{th} = \frac{\varepsilon'_{r-rev}}{\alpha'_r}, \qquad (6)$$

At $\omega = 1$ rad/s, the threshold field is near 5 kV/cm for both materials, which is higher to what is obtained in the literature for lead zirconate titanate thin films [18]. The little size of the residual ferroelectric clusters into the antiferroelectric matrix avoids the domain wall motions,

thus, the energy necessary to unpinning is more important [3,24]. According to Boser, the thershold field is proportional to:

$$E_{th} \propto \frac{\sqrt{NF_1}}{f_0 P_{FE}}, \quad (7)$$

where f_0 is a geometrical factor depending on the domain wall type (90° or 180°), P_{FE} is the polarization of the cell, N is the number of obstacles and F_1 is a function which is proportional to the pinning depth of the obstacle. The value P_{FE} of the polarization do not depend on the orientation of the cell (Fig. 3). For the two samples, the threshold field are then closed which means that the same type of defects take place in both materials, as mentioned previously. The $PbZrO_3$ with different crystallographic direction has then the higher threshold field due to more obstacles N.

The $PbZrO_3$ with different crystallographic direction presents also a higher vibrational dissipation factor ($m_{rev} = \varepsilon''_{f\text{-}rev} / \varepsilon'_{f\text{-}rev} = 0.23$) due to a greater interaction between the walls when the ferroelectric domain walls density is higher [20]. However these values are lower to what is reported in the literature for ferroelectric materials ($m_{rev} \geq 0.35$) [25] due to small residual ferroelectric cluster well distributed into the antiferroelectric matrix [3].

The pinning dissipation factor ($m_\alpha = \alpha_f'' / \alpha_f' = 0.25$) of the $PbZrO_3$ sample with different crystallographic direction is then higher than the dissipation factor of the (100) $PbZrO_3$ for the same reason than $m_{rev.}$ and these coefficients are also lower than what is reported in the literature ($m_\alpha \geq 0.31$ [25-26]) according to weak interaction between domain walls in the residual ferroelectric state.

Conclusion

Antiferroelectric materials are intensively study for the energy storage applications in both the academic and industry communities. Recently, ferroelectric domain walls have been located in antiferroelectric phase. This domain walls created supplementary dielectric losses and may disadvantage the desired applications. In this study, two $PbZrO_3$ samples have been studied: one with a (100) preferential orientation and one with two different crystallographic direction ((100) and (111)). The sample with the (111) direction has a higher polarization and lower field transitions due to the reduction of the angle between the applied electric field and the ferroelectric polar axis ($\vec{P}_{FE}$). However, to obtain this orientation, a 2nm Ti seed layer has been used and the oxidation of this layer during the $PbZrO_3$ process generates oxygen vacancies, which increases the hopping conduction. The dissipation factors at low frequency tan δ_{lf} of the $PbZrO_3$ with different crystallographic direction are then more important. This sample presents also a higher correlation of dipoles ($|S_{hf}| = 0.007$) due to the energy gain associated with their orientation. For the (111) orientation, the energy necessary to head-to-tail dipoles (antiferroelectric state) to switch to parallels dipoles (ferroelectric state) is lower than for the (100) orientation. Consequently, The (100) $PbZrO_3$ sample has a lower value of $|S_{hf}|$ (= 0.005) due to a higher energy necessary (higher transition field E_{AF}) for the transitions of head-to-tail dipoles.

For the ferroelectric domain walls, the real part of the vibration and pinning coefficients of the $PbZrO_3$ with different crystallographic direction are higher compared to the (100) $PbZrO_3$. These two coefficients are proportional to the domain wall density and the $PbZrO_3$ with different crystallographic direction has more inhomogeneity of the crystallization orientation and consequently more nucleation site for domain walls. The other coefficients are then nearly the same because the crystallization conditions are identical and the differently oriented domain

walls thus have the same environment (same grain size and similar defects in the two samples) and interact in the same way.
In order to obtain an easily switching material, the (111) crystallographic orientation seems to be better. The crystallization conditions will then influence the extrinsic properties of the material (hopping conduction and dielectric losses). For identical crystallization conditions, the domain walls are not influenced by the crystallization direction, the same type of walls are obtained on the $PbZrO_3$ sample (100) as on the sample with different crystallographic orientations. Only the wall density is modified.

References

[1] P. Sharma *et al.*, « Nonvolatile ferroelectric domain wall memory », *Sci. Adv.*, vol. 3, nº 6, p. e1700512, juin 2017, doi: 10.1126/sciadv.1700512.

[2] C. Borderon, K. Nadaud, M. Coulibaly, R. Renoud, et H. Gundel, « Mn-Doped $Ba_{0.8}Sr_{0.2}$ TiO 3 Thin Films for Energy Storage Capacitors », p. 10.

[3] M. D. Coulibaly, C. Borderon, R. Renoud, et H. W. Gundel, « Enhancement of $PbZrO_3$ polarization using a Ti seed layer for energy storage application », *Thin Solid Films*, vol. 716, p. 138432, déc. 2020, doi: 10.1016/j.tsf.2020.138432.

[4] R. Xu *et al.*, « Ferroelectric polarization reversal via successive ferroelastic transitions », *Nat. Mater.*, vol. 14, nº 1, p. 79-86, janv. 2015, doi: 10.1038/nmat4119.

[5] H. Wu, X. Ma, Z. Zhang, J. Zeng, J. Wang, et G. Chai, « Effect of crystal orientation on the phase diagrams, dielectric and piezoelectric properties of epitaxial $BaTiO_3$ thin films », *AIP Adv.*, vol. 6, nº 1, p. 015309, janv. 2016, doi: 10.1063/1.4940205.

[6] Y. Zhao, H. Gao, X. Hao, et Q. Zhang, « Orientation-dependent energy-storage performance and electrocaloric effect in PLZST antiferroelectric thick films », *Mater. Res. Bull.*, vol. 84, p. 177-184, déc. 2016, doi: 10.1016/j.materresbull.2016.08.005.

[7] W. Zhu, W. Ren, H. Xin, P. Shi, et X. Wu, « Enhanced ferroelectric properties of highly (100) oriented $Pb(Zr_{0.52}Ti_{0.48})O_3$ thick films prepared by chemical solution deposition », *J. Adv. Dielectr.*, vol. 03, nº 02, p. 1350011, avr. 2013, doi: 10.1142/S2010135X13500112.

[8] G.-T. Park, J.-J. Choi, C.-S. Park, J.-W. Lee, et H.-E. Kim, « Piezoelectric and ferroelectric properties of 1-µm-thick lead zirconate titanate film fabricated by a double-spin-coating process », *Appl. Phys. Lett.*, vol. 85, nº 12, p. 2322-2324, sept. 2004, doi: 10.1063/1.1794354.

[9] K. G. Brooks, I. M. Reaney, R. Klissurska, Y. Huang, L. Bursill, et N. Setter, « Orientation of rapid thermally annealed lead zirconate titanate thin films on (111) Pt substrates », *J. Mater. Res.*, vol. 9, nº 10, p. 2540-2553, 1994.

[10] T. Tani, J. Li, D. Viehland, et D. A. Payne, « Antiferroelectric-ferroelectric switching and induced strains for sol-gel derived lead zirconate thin layers », *J. Appl. Phys.*, vol. 75, nº 6, p. 3017-3023, mars 1994, doi: 10.1063/1.356146.

[11] S.-Y. Chen, I.-W. Chen, et others, « Texture development, microstructure evolution, and crystallization of chemically derived PZT thin films », *J. Am. Ceram. Soc.*, vol. 81, nº 1, p. 97–105, 1998.

[12] J. Ge, D. Remiens, J. Costecalde, Y. Chen, X. Dong, et G. Wang, « Effect of residual stress on energy storage property in $PbZrO_3$ antiferroelectric thin films with different orientations », *Appl. Phys. Lett.*, vol. 103, nº 16, p. 162903, oct. 2013, doi: 10.1063/1.4825336.

[13] K. Boldyreva, D. Bao, G. Le Rhun, L. Pintilie, M. Alexe, et D. Hesse, « Microstructure and electrical properties of (120)O-oriented and of (001)O-oriented epitaxial antiferroelectric PbZrO3 thin films on (100) SrTiO3 substrates covered with different oxide bottom electrodes », *J. Appl. Phys.*, vol. 102, nº 4, p. 044111, août 2007, doi:

10.1063/1.2769335.
[14] L. Pintilie, K. Boldyreva, M. Alexe, et D. Hesse, « Coexistence of ferroelectricity and antiferroelectricity in epitaxial PbZrO3 films with different orientations », *J. Appl. Phys.*, vol. 103, nº 2, p. 024101, janv. 2008, doi: 10.1063/1.2831023.
[15] C. Borderon, R. Renoud, M. Ragheb, et H. W. Gundel, « Description of the low field nonlinear dielectric properties of ferroelectric and multiferroic materials », *Appl. Phys. Lett.*, vol. 98, nº 11, p. 112903, 2011, doi: 10.1063/1.3567777.
[16] D. V. Taylor and D. Damjanovic, "Evidence of domain wallcontribution to the dielectric permittivity in PZT thin films at subswitching fields", J. Appl. Phys., 82, pp. 1973-1975, 1997.
[17] K. Vaideeswaran, K. Shapovalov, P. V. Yudin, A. K. Tagantsev, et N. Setter, « Moving antiphase boundaries using an external electric field », *Appl. Phys. Lett.*, vol. 107, nº 19, p. 192905, nov. 2015, doi: 10.1063/1.4935122.
[18] C. Borderon, R. Renoud, M. Ragheb, et H. W. Gundel, « Dielectric long time relaxation of domains walls in PbZrTiO3 thin films », *Appl. Phys. Lett.*, vol. 104, nº 7, p. 072902, févr. 2014, doi: 10.1063/1.4866156.
[19] A. K. Jonscher, « Dielectric relaxation in solids », *J. Phys. Appl. Phys.*, vol. 32, nº 14, p. R57, 1999.
[20] K. Nadaud, C. Borderon, R. Renoud, et H. W. Gundel, « Effect of manganese doping of BaSrTiO3 on diffusion and domain wall pinning », *J. Appl. Phys.*, vol. 117, nº 8, p. 084104, 2015.
[21] C. Slouka *et al.*, « The Effect of Acceptor and Donor Doping on Oxygen Vacancy Concentrations in Lead Zirconate Titanate (PZT) », *Materials*, vol. 9, nº 12, p. 945, nov. 2016, doi: 10.3390/ma9110945.
[22] A. K. Jonscher, *Dielectric Relaxation in Solids*. Chelsea Dielectrics Press, 1983.
[23] M. I. Morozov et D. Damjanovic, « Charge migration in Pb(Zr,Ti)O3 ceramics and its relation to ageing, hardening, and softening », *J. Appl. Phys.*, vol. 107, nº 3, p. 034106, févr. 2010, doi: 10.1063/1.3284954.
[24] S. K. Singh, N. Menou, H. Funakubo, K. Maruyama, et H. Ishiwara, « (111)-textured Mn-substituted BiFeO3 thin films on SrRuO3/Pt/Ti/SiO2/Si structures », *Appl. Phys. Lett.*, vol. 90, nº 24, p. 242914, juin 2007, doi: 10.1063/1.2748323.
[25] C. Borderon, A. E. Brunier, K. Nadaud, R. Renoud, M. Alexe, et H. W. Gundel, « Domain wall motion in Pb(Zr0.20Ti0.80)O3 epitaxial thin films », *Sci. Rep.*, vol. 7, nº 1, déc. 2017, doi: 10.1038/s41598-017-03757-y.
[26] J. E. García, R. Pérez, et A. Albareda, « Contribution of reversible processes to the non-linear dielectric response in hard lead zirconate titanate ceramics », *J. Phys. Condens. Matter*, vol. 17, nº 44, p. 7143-7150, nov. 2005, doi: 10.1088/0953-8984/17/44/007.